RSC Advances

PAPER

View Article Online
View Journal | View Issue

Cite this: *RSC Adv.*, 2020, **10**, 20118

Mussel inspired ZIF8 microcarriers: a new approach for large-scale production of stem cells

Mahsa Asadniaye Fardjahromi,[ab] Amir Razmjou,[cd] Graham Vesey,[e] Fatemeh Ejeian,[cf] Balarka Banerjee,[e] Subhas Chandra Mukhopadhyay[a] and Majid Ebrahimi Warkiani *[bg]

Metal–organic frameworks (MOFs) have high porosity, large surface area, and tunable functionality and have been widely used for drug loading. The aim of this study was to exploit unique features of zeolitic imidazolate framework-8 (ZIF8) to develop an innovative composite microcarrier (MC) for human mesenchymal stem cells (hMSCs) adhesion and proliferation. ZIF8 MCs were prepared by immobilization of polydopamine/polyethyleneimine (PDA/PEI) and ZIF8 on the surface of polystyrene beads. The chemical properties of MCs such as coating stability and homogeneity were characterized by different techniques such as ATR-FTIR, XRD, EDX, SEM, and contact angle. The prepared MCs were tested using human adipose-derived mesenchymal stem cells (hADSCs) in both static and dynamic conditions, and results were compared to a commercially available MC (Star-Plus), polydopamine coated MCs and amine-functionalized MCs as a control. Results show that PDA/PEI/ZIF8 coated MCs (in short: ZIF8 MCs) provides an excellent biocompatible environment for hADSCs adhesion and growth. In conclusion, ZIF8 MCs represent suitable and low-cost support for hADSCs culture and expansion, which can maximize cell yield and viability while preserving hADSCs multipotency. The present findings have revealed this strategy has the potential for chemical and topographical modification of MCs in tissue engineering applications.

Received 6th May 2020
Accepted 12th May 2020

DOI: 10.1039/d0ra04090h

rsc.li/rsc-advances

1 Introduction

Human mesenchymal stem cells (hMSCs) are unique cells with the capacity to differentiate into new cell types with specific functionalities such as adipocyte, chondrocyte, and osteoblasts.[1,2] As such, hMSCs have emerged as a promising candidate in tissue engineering, cell therapy, and regenerative medicine.[3–10] This is due to their ease of isolation, immunomodulatory effects, and multipotency.[11] For instance, hMSCs-based therapies are able to supplement many of the body's natural disease responses in patients who suffer from a wide range of diseases such as cartilage and bone damage, cancer, diabetes, autoimmune diseases, and spinal cord injuries.[12–16]

HMSCs can be isolated from many sources such as adipose tissue, dermal tissue, intervertebral disc, dental tissues, human placenta, cord blood, *etc.*[17] However, cell sourced from different donors suffer from high levels of population heterogeneity, and the number of extracted cells are typically inadequate for cell-based therapies (10^6 to 10^9 cells per kg of a patient).[18] A large-scale production method to yield sufficient hMSCs of uniform quality would greatly benefit the cost per treatment and efficiency of clinical strategies.

Current 2D cell culture methods on single or multilayer platforms such as T flasks and multilayer flasks are labor-intensive operation and possess limited space for large cell expansion. An alternative approach is microcarrier (MC)-based bioreactor systems, in which cells grow in a suspension of MCs and culture media in stirred bioreactors.[19–21] MCs are typically spherical particles in size range of 100–300 μm, providing large surface area to volume ratio for expanding anchorage-dependent cells.[22–24] MC-based cultivation systems benefit from scalability, superior control of culture parameters (*e.g.*, pH, gas exchange, nutrient consumption), and homogenous culture conditions,[25] which consequently lead to improved cell yield and proliferation capacity compared with 2D cell culture. In addition to the application of MCs in stem cell production, MCs have been used in amplifying various cell types with preserving their phenotype for tissue regeneration. In

[a]*School of Engineering, Macquarie University, Sydney, NSW, 2109, Australia*
[b]*School of Biomedical Engineering, University of Technology Sydney, Sydney, NSW, 2007, Australia. E-mail: majid.warkiani@uts.edu.au*
[c]*Department of Biotechnology, Faculty of Biological Science and Technology, University of Isfahan, Isfahan, 73441-81746, Iran*
[d]*UNESCO Centre for Membrane Science and Technology, School of Chemical Engineering, University of New South Wales, Sydney, NSW, 2052, Australia*
[e]*Regeneus Ltd, Paddington, Sydney, NSW, 2021, Australia*
[f]*Department of Cellular Biotechnology, Cell Science Research Center, Royan Institute for Biotechnology, ACECR, Isfahan, Iran*
[g]*Institute of Molecular Medicine, Sechenov First Moscow State University, Moscow 119991, Russia*

addition, MCs play a key role in delivery of therapeutic molecules to the damaged tissues.[26,27]

Since the first reported fabrication of MCs,[28] many attempts have been made to manipulate surface chemistry and morphological trait of MCs to regulate cell signalling pathways and consequently achieve higher cell attachment, growth, and differentiation.[29] Currently, the vast majority of MCs available in the market are made of glass or synthetic biodegradable polymers[18] which need further modification for enhancing cell attachment. A common strategy for improving cell attachment is using natural polymers and ECM proteins such as laminin, vitronectin, fibronectin, heparin, hyaluronic acid, collagen, and gelatin during MCs fabrication.[19,27] However, natural polymers are structurally weak and susceptible to damage from agitation and fluid shear.[30–32]

To fabricate appropriate MCs with higher mechanical stability in tissue engineering, studies have focused on the selection of synthetic biomaterial with specific chemical properties and morphology to direct stem cell fate. To illustrate, ceramics containing calcium ions (Ca^{2+}) and phosphate anions have been used in the fabrication of MCs to enhance osteogenic differentiation and proliferation of bone cells.[33] The design of MCs with micro-nano roughness or porous structure results in higher cell adhesion, differentiation, and therapeutic drug loading capacity.[33–37] Nonetheless, all these methods need to change the bulk properties of MCs which is costly, time-consuming, and hard to synthesize and may not give the desired surface property required for directing stem cell fate. Therefore, developing a facile method for surface engineering of MCs with the synthetic material with high mechanical stability, biocompatibility, and proliferation yield is necessary.

Zeolitic imidazolate frameworks (ZIFs), a subclass of metal–organic frameworks, are hybrid materials constructed by tetrahedral building blocks in which metal ions (M = Co and Zn) connect to nitrogen atoms of imidazole-derived ligands. This class of porous materials has proven applicable in various areas such as gas sensing, gas storage, and catalysis[38–40] due to their microporous network structure, high thermal and mechanical stabilities, chemical functionality, and high surface area. Besides, size, morphology, structure, and surface chemistry of ZIFs can be tailored through a variety of approaches including post-synthesis modification and changing synthetics parameters.[41–43] Studies have demonstrated these novel functional materials are a promising candidate for coating and protecting cells and bio-entities from external environments such as heat, mechanical stress, UV irritation, *etc.*[44–46] In addition to that, large loading capacity, biocompatibility, biodegradability, stimuli-responsivity, and versatile morphologies of ZIFs

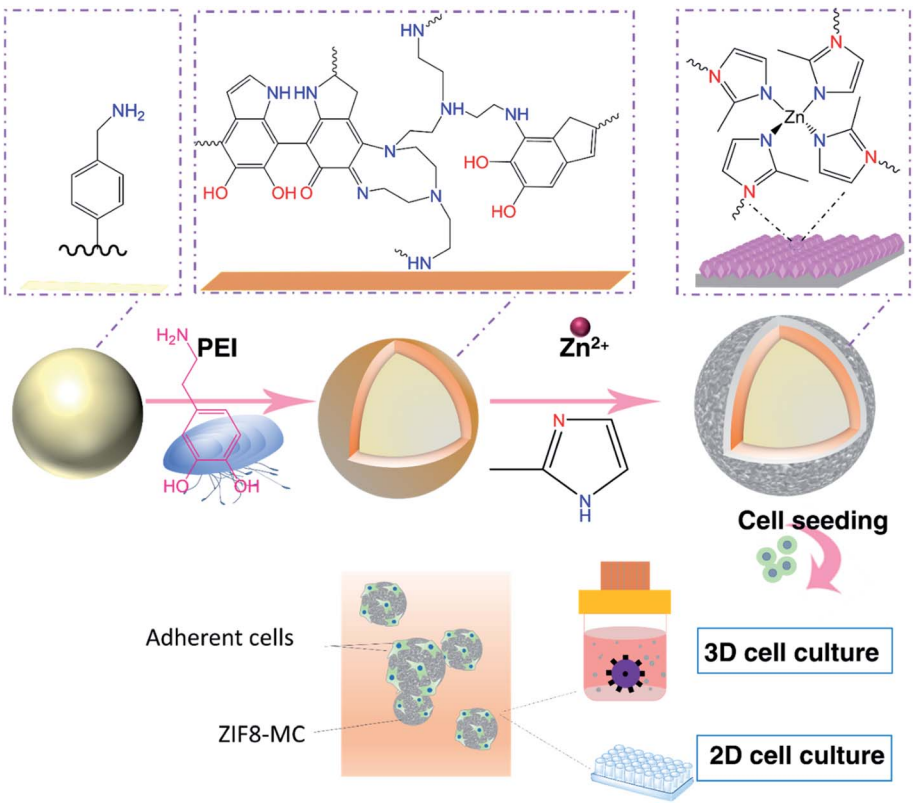

Scheme 1 Schematic fabrication of bioinspired MCs and expansion of hADSCs in static and dynamic conditions. PDA MCs were synthesized by immersing PS beads on Tris base buffer solution in the presence of PEI and DA·HCl. ZIF8 MCs, then fabricated by 3D coating ZIF8 thin film on the surface of PDA MCs in a solution containing (2-MIM) and $Zn(NO_3)_2$. Cell culture was studied with two methods: static two-dimensional (2D), and three-dimensional dynamic (3DD). In the static method, hADSCs were seeded on MCs in 24-well ultra-low attachment plate and cultured for 7 days. On the dynamic condition, cell culture has been performed in PBS bioreactor and the suspension of hADSCs and MCs were stirred for 7 days.

materials enable them to serve as nanocarriers in clinical tumor therapy and drug delivery systems.[46–48] As a result, these unique qualities make ZIFs materials ideally suited to tuning surface properties of MCs.

Herein, for the first time, we have proposed a facile method for surface engineering of MCs using biocompatible and tunable ZIF8 thin film layers (Scheme 1). In this approach, non-treated MCs (polystyrene beads) were modified with ZIF8/polydopamine/polyethyleneimine layer (ZIF8 MCs). A polydopamine/polyethyleneimine (PDA/PEI) coating was applied to induce heterogeneous nucleation and growth of ZIF8 film with high mechanical stability on the surface of polystyrene beads.[49,50] In this study, we showed that ZIF8 coating is biocompatible and can change the surface properties of MCs such as surface chemistry, hydrophilicity, surface charge, surface free energy, and roughness. These changes affected cell behaviors in a positive manner and enhanced cell attachment and proliferation of human adipose stem cells (hADSCs) in both 2D and 3D conditions. Thus, this method can be applied as a potential method for tailoring the physicochemical properties of MCs in tissue engineering and cell therapy.

2 Experimental section

2.1. Fabrication of MCs

2.1.1 Materials and reagents. Dopamine hydrochloride acid (DA·HCl), tris(hydroxymethyl) aminomethane (Tris base), aminomethyl polystyrene beads (PS beads) (1–1.5 mmol g^{-1} N loading), polyethyleneimine (PEI), 2-methylimidazole (2-MIM), zinc nitrate, were purchased from Sigma Aldrich. Ethanol was obtained from Chem-supply Australia. Star-Plus MCs (Pall, SoloHill) were purchased from Pall Biotech. PDA MCs and ZIF8 MCs were fabricated according to the following procedures.

2.1.2 Preparation of PDA MCs. PDA MCs were fabricated according to the following procedure. First, 1 g PS beads were washed with ethanol and dispersed in a dopamine solution (2 mg ml^{-1} DA·HCl in 10 mM Tris base buffer solution, pH 8.5) and PEI (1000 MW, 2 mg ml^{-1}). The mixture was shaken gently by an orbital shaker. The colour of the solution changed gradually from colourless to dark brown during the reaction, indicating the oxidation of dopamine monomers and formation of a uniform PDA layer on the surface of beads. The shaking was continued for 16 h. Next, PDA coated PS beads were washed with water several times and sonicated to remove excess PDA. Finally, MCs were washed with ethanol and dried in a stream of N_2.

2.1.3 Preparation of ZIF8 MCs. ZIF8 MCs were fabricated by coating a layer of ZIF8 on the surface of PDA MCs according to our previous report.[49] An aqueous solution of zinc nitrate ($Zn(NO_3)_2$) (2.74 mg ml^{-1}), gradually added to the solution of 2-MIM (56.6 mg ml^{-1}). The mixture turned to white cloudy after agitation. Afterwards, 1 g of PDA MCs were immersed in the mixture. The reaction was left at room temperature for two hours. Finally, MCs were rinsed with DI water and ethanol several times and dried in a stream of N_2.

2.2. Characterization of MCs

ATR-FTIR spectra were recorded by Thermo scientific Nicolet 6700ATR spectrophotometer. Images of MCs were taken by light microscopy (Olympus CKX53). Scanning electron microscopy (SEM) images and energy-dispersive X-ray spectroscopy (EDX) were recorded by Zeiss Supra 55VP microscope. Before taking SEM images and EDX analysis, samples were coated with gold–palladium with a thickness of 15 nm. The surface area of MCs was determined by SA-9600 BET Surface analyser by adsorption of gas (N_2 at 77 K) *via* Brunauer–Emmett–Teller theory. The surface charge of MCs was measured using a Zeta sizer Nano ZS Malvern Instruments Ltd. The X-ray powder diffraction (XRD) pattern of ZIF8 crystals was taken by Bruker D8 Discover XRD for 2θ from 4 to 36° (0.026° step size). In order to ease the process of contact angle measurement and atomic force microscopy (AFM) imaging, tissue culture plate (TCP) was chosen as a base material for evaluating surface properties of PDA/PEI and ZIF8/PDA/PEI coating since TCP and control groups are made of polystyrene, and they have similar chemical property. Water wettability and surface free energy of (TCP), PDA/PEI coated on TCP (PDA-TCP), and ZIF8/PDA/PEI coated on TCP (ZIF8-TCP) were evaluated with Kruss Drop Shape Analyser. PDA-TCP and ZIF8-TCP were synthesised according to the procedures mentioned in the Fabrication of MCs. Surface free energy was calculated according to the acid–base (van-Oss) approach by using three liquids (formamide, water, and glycerol). Surface topography of TCP, PDA-TCP, and ZIF8-TCP was performed in tapping mode by using AFM (Park XE7 AFM).

2.3. Culture of hADSCs on MCs

Primary hADSCs were initially expanded and characterized by Regeneus Pty Ltd, Australia. The cryopreserved cells (passage 6) obtained from the company were thawed and cultured in αMEM medium supplemented with 10% FBS and 1% penicillin/streptomycin (Gibco). All the cells used in this study were in the passage 6–10. To investigate the impact of ZIF8 coating on cell attachment and growth, cell seeding was conducted with three types of MCs. A market MC (Star-Plus MCs) due to its positive charge and high capability in cell proliferation was utilized as a positive control. Other MCs (PS beads and PDA MCs) were used to compare the efficiency of cell attachment and growth before and after ZIF8 coating. Prior to cell seeding, PS beads, PDA, and ZIF8 MCs, they were immersed in ethanol 70% (v/v) for 1 hour and then exposed UV for 30 min. Star-Plus MCs were sterilized using an autoclave according to the manufacturer's instructions. MCs were incubated in culture medium for 12 hours before cell seeding.

2.3.1 Static culture condition. hADSCs were seeded and incubated at 37 °C in a humidified atmosphere containing 5% CO_2. After cells reached 80% confluence, they were harvested by TryplE™ select (1×) (Gibco). Cells were seeded at the density of 10^4 cells per mg of each type of MCs in the ultra-low adherent culture dishes (corning). Every two days, 80% percentage of culture medium was aspirated and replaced with an equal volume of fresh medium. To investigate cell attachment and growth, a sample of the MCs was taken at the 1st, 3rd, and 7th day

of cell culture and analyzed by fluorescent microscopy after DAPI staining. Accordingly, cells on the surface of the MCs were fixed with paraformaldehyde 4% (Sigma Aldrich) and stained with DAPI (Invitrogen™). Images were taken with a fluorescent microscope (Olympus DP80).

2.3.2 Dynamic culture condition. 3D cell culture was performed in a100 ml PBS mini bioreactor (PBS biotech). All MCs were sterilized according to the procedure described in 2D cell culture. The equal amount (1 g) of each MC were separately equilibrated at culture media overnight at 37 °C before cell seeding. hADSCs at a density of 1.5×10^6 cells per g MCs were added into separate PBS mini bioreactors. The bioreactor was initially operated at a speed of 15 rpm for the first 25 h to enhance cell attachment. After this period, the speed was increased to 22 rpm to obtain near-full suspension of cell-bound MCs.

2.4. Confocal microscopy images

To observe the MCs occupancy by hADSCs on different days, samples on the 1st, 3rd, and 7th day of cell culture were washed with PBS twice and fixed with 4% (v/v) paraformaldehyde for 20 min. Then MCs were immersed in 0.2% Triton X-100 for 10 min. Finally, MCs were washed with PBS buffer and stained with DAPI. Samples were examined with a confocal microscope (Olympus FV3000RS).

2.5. Cell proliferation assay

The impact of PDA and ZIF8 MCs on cell growth was evaluated by using MTS colorimetric assay. Samples from all MCs on day 1, 3, and 7 were washed with PBS twice, and MTS assay protocol was conducted according to the kit instruction (Sigma-Aldrich). Absorbance was measured at 490 nm using a Tecan Spark multimode microplate reader.

2.6. Cell harvesting

On the 7th day of culture, MCs were rinsed with PBS and detached by incubating in TryplE for 15 min. The suspension was gently pipetted multiple times to assist cell dissociation. The process of separating the MCs from cells was conducted by pouring the suspension of MCs and beads through a sterile strainer (Corning cell strainer 100 μm, Sigma-Aldrich, Australia) and washing MCs with PBS several times. The filtrate contained cells were centrifuged, and the total number of viable cells on each MC was measured by staining cells with trypan blue dye (Gibco™) and counted by hemocytometer.

2.7. Adipogenic and osteogenic differentiation capability

The hADSCs cells harvested from bioreactor were seeded into 24-well plate to confirm differentiation capacity. After three days, the normal growth medium was replaced with 500 μl specific adipogenic or osteogenic differentiation medium (StemPro™ Adipogenesis/Osteogenesis Differentiation Kit). Every three days, the media was refreshed. The plate was maintained at 37 °C in a humidified atmosphere containing 5% CO_2 incubator for 21 days. Differentiation capability of cells to adipocytes and osteoblasts were studied by Oil Red O and Alizarin Red S staining.

2.7.1 Oil Red O staining. The cells treated with adipogenic differentiation media were washed twice with Ca^{2+} and Mg^{2+} free DPBS twice. Cells then were fixed by adding 4% formaldehyde and incubation at room temperature. Oil Red O solution was prepared according to the following procedure. 300 mg of Oil Red O (Sigma-Aldrich) was dissolved in 10 ml 2-propanol. Next, 9 ml of Oil Red O solution was added to 6 ml deionized water, and the mixture was left at room temperature for 10 min. The obtained solution then was filtered through a 0.2 μm filter (Minisart®, Sartorius Stedim Biotech). After 1 hour, wells were rinsed with deionized water and stained with 1 ml Oil Red O solution for 30 min at room temperature.

2.7.2 Alizarin Red S staining. The cells treated with osteogenic differentiation media were fixed with 70% ethanol for 1 hour, followed by washing deionized water. The cells were incubated with 500 μl of 2% solution of Alizarin Red S (Sigma Aldrich) in deionized water at pH 4.2 at room temperature. After 1 hour, excess dyes aspirated and washed with water several times. Finally, light microscopy images were taken from random locations.

2.8. Statistical analyses

Experiments were carried out at least three times. All statistical analyses were performed with by one-way ANOVA test by using GraphPad Prism analysis program.

3 Result and discussion

3.1. Characterization of ZIF8 MCs

PDA MCs were synthesized by oxidation polymerization of DA in an alkaline solution. To obtain a uniform PDA coating on the surface of beads, PEI was added during DA polymerization. The first identification of oxidative dopamine polymerization is a visible color change in PS beads from pale white to dark brown (Fig. 1A and B). One of the advantages of PDA MCs is that the surface of the MCs are still reactive and can post modify *via* Schiff base and Michael addition.[51] Furthermore, PDA is a reducing and stabilizing agent facilitating the heterogeneous nucleation and growth of ZIFs. To be more precise, in order to design ZIF8 MCs for 3D cell culture, the ZIF8 layer on the surface of beads should not be fragile and can tolerate the shear stress and agitation inside the bioreactor. *In situ* and secondary growth of ZIF8 on the surface of the non-coating beads does not allow ZIF8 crystals to adhere tightly to the beads. PDA layers consist of amines and imine groups, which are similar to imidazole organic ligands, provide abundant sites for nucleation and chelation of ZIF8.[52] Hence, ZIF8 MCs were synthesized by first coating PS beads with PDA/PEI and then creating a thin layer of ZIF8. After ZIF8 coating, the color changes between PDA and ZIF8 MCs was insignificant (Fig. 1C). AFM analysis (Fig. 1D and E) revealed that after coating PDA/PEI on TCP, the surface becomes smoother, such a way that the roughness parameters changed from $Sa = 16.99 \pm 3.35$ nm to $Sa = 3.75 \pm 0.51$ nm. However, ZIF8 coating increased the

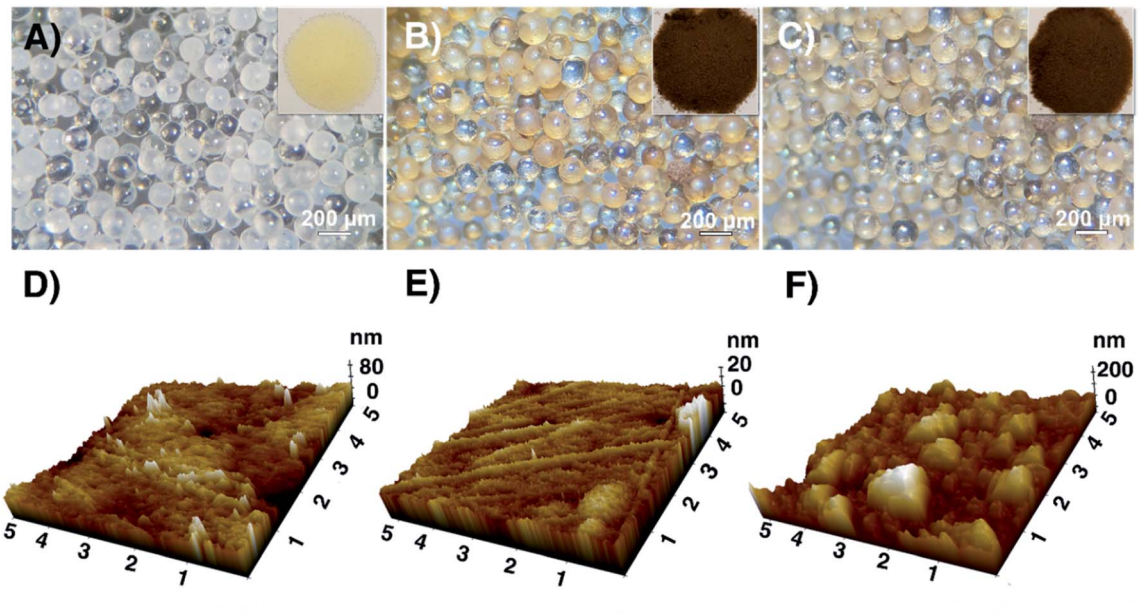

Fig. 1 Light microscopy images of (A) PS beads, (B) PDA MCs, (C) ZIF8 MCs. Digital images of each sample are presented as inset color of PS beads changed to dark brown after coating with PDA. 3D AFM topographical images of (D)TCP, (E) PDA-TCP, (F) ZIF8-TCP. Surface roughness changed after coating PDA/PEI and PDA/PEI/ZIF8 on the surface of TCP.

roughness value significantly to Sa = 40.42 ± 2.01 nm due to the crystal structure of ZIF8 thin film (Fig. 1F).

FTIR spectrum of PDA MCs (Fig. 2A) indicates C=C stretching at 1609 cm^{-1} from indole ring bonds, N–H bending at 1510 cm^{-1}, and C=O and C–O bonds at 1700 cm^{-1} and 1284 cm^{-1}. Another peak arising at 1647 cm^{-1} can be attributed to C=N bonds due to the Schiff base reaction between PEI and PDA during the coating. The peak at 422 cm^{-1} can be ascribed to the stretching of Zn–N bond during the ZIF8 formation in which tetrahedral Zn^{2+} ions are linked by nitrogen ligands (2-MIM ligands). The crystal structure of ZIF8 MCs was evaluated with XRD (Fig. 2B). X-ray diffraction of PS beads and PDA

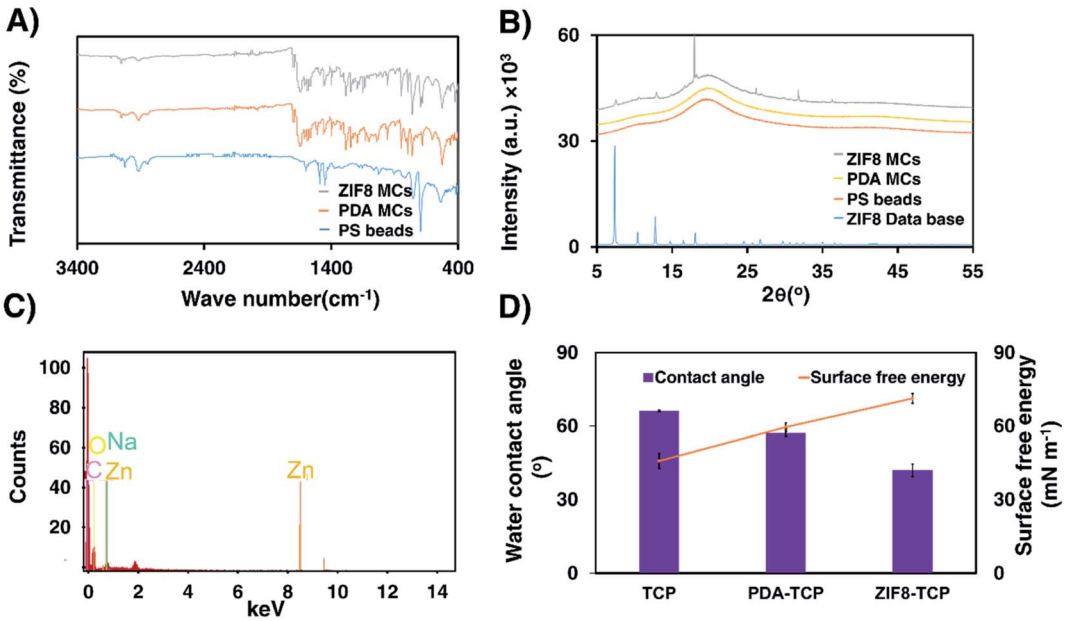

Fig. 2 Characterization of PDA MCs and ZIF8 MCs. (A) ATR-FTIR spectra of PS beads, PDA MCs and ZIF8 MCs. (B) XRD patterns of PS beads, PDA MCs, ZIF8 MCs, and ZIF8 database. (C) Energy dispersive spectra (EDX) of ZIF8 MCs. (D) Water contact angle and surface free energy measurement of TCP, PDA-TCP and ZIF8-TCP with diiodomethane, water and glycerol using Van Oss method. Each sample was assessed in three replicates.

Table 1 Surface area and zeta potential of MCs

MCs	BET surface area ($m^2 g^{-1}$)	Z potential (mV)
PS beads	1.8277	29
PDA MCs	2.3200	−36.9
ZIF8 MCs	8.6640	−17.6
Star-Plus MCs	0.4487	33.2

MCs indicates no crystal structure. However, after a ZIF8 thin film formed on the surface of PDA MCs, the characteristic peaks of ZIF8 could be observed in XRD spectrum. These XRD peaks along with the presence of Zn peaks in the EDX spectrum of ZIF8 MCs supports the formation of a layer containing Zn on the surface of the beads (Fig. 2C). Water contact angle and surface free energy of the substrate varied noticeably by coating PDA and ZIF8 as a consequence of modified surface chemistry. Fig. 2D shows the surface wettability of TCP after coating with PDA dropped from 66.2° to 57.3°, and surface free energy of TCP raised from 45.8 to 59.6 mN m^{-1} as a result of abundant hydroxyl groups on the surface of PDA-TCP. Coating a ZIF8 thin film layer on the surface of PDA-TCP increased the hydrophilicity significantly, making it the most hydrophilic coating group with the contact angle of 42° and the highest surface free energy (71.3 mN m^{-1}). Increased ZIF8 coating wettability may result from the higher surface roughness of the TCP, which in turn leads to an enlarged surface area and increased hydrophilicity and adhesion according to Wenzel equation.[53]

The zeta potential of different MCs in aqueous solution (pH = 7) are shown in Table 1. After PDA coating the zeta potential changed from −29 mV to −36.9 mV due to the deportation of phenolic groups of PDA at a pH = 7.[54] The observed change in zeta potential indicates polymerization of PDA on the surface of PS beads successfully. It has been shown that the isoelectronic point of ZIF8 occurs at a pH of 9.8, and the surface charge of ZIF8 for the pH below 9.8 has positive values.[55] When PDA MCs are coated with ZIF8, the positive charge of ZIF8 increased the zeta potential value to −17.6 mV. Nitrogen adsorption–desperation isotherm of MCs is shown in Table 1. The BET surface area of PS beads raised slightly from 1.8277 $m^2 g^{-1}$ to 2.3200 $m^2 g^{-1}$ after coating with PDA. Interestingly, ZIF8 coating increased the surface area of PDA MCs to 8.6 $m^2 g^{-1}$ due to the microporous structure of the ZIF8 layer on the surface of the beads. The surface morphology of PDA and ZIF8 MCs was evaluated with SEM. It can be observed that the morphology of PS beads did not noticeably change after coating PDA/PEI (Fig. 3B1–B3). However, after coating ZIF8, the roughness has been increased, and a homogenous and compact ZIF8 nanoparticle film on the surface of PS beads were formed (Fig. 3C1–C3).

3.2. hADSCs culture in the stationary condition

To achieve higher stem cell yield and differentiation, we hypothesized that ZIFs is a promising candidate for fabrication of MCs due to their large surface area, biocompatibility, mechanical stability, and high tunability. In order to prove ZIF8 MCs are suitable for 3D upscaling of stem cell production, first,

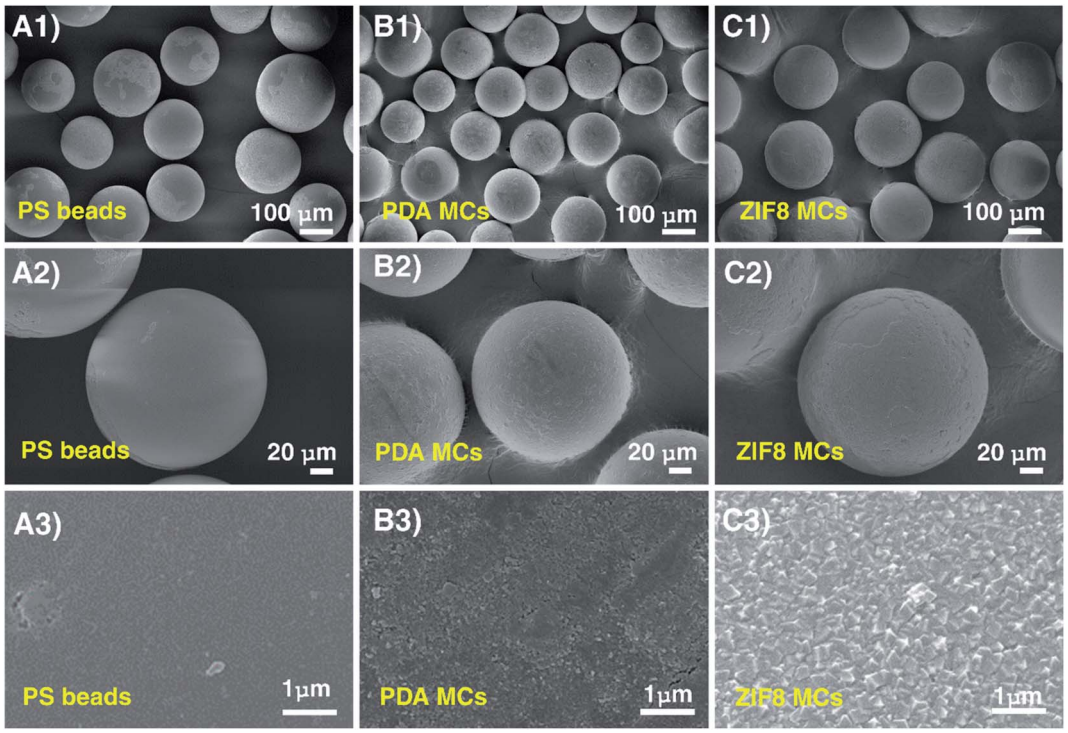

Fig. 3 SEM images of PS beads (A1–A3), PDA MCs (B1–B3), ZIF8 MCs (C1–C3). Surface roughness increased by coating ZIF8/PDA/PEI on the surface of PS beads.

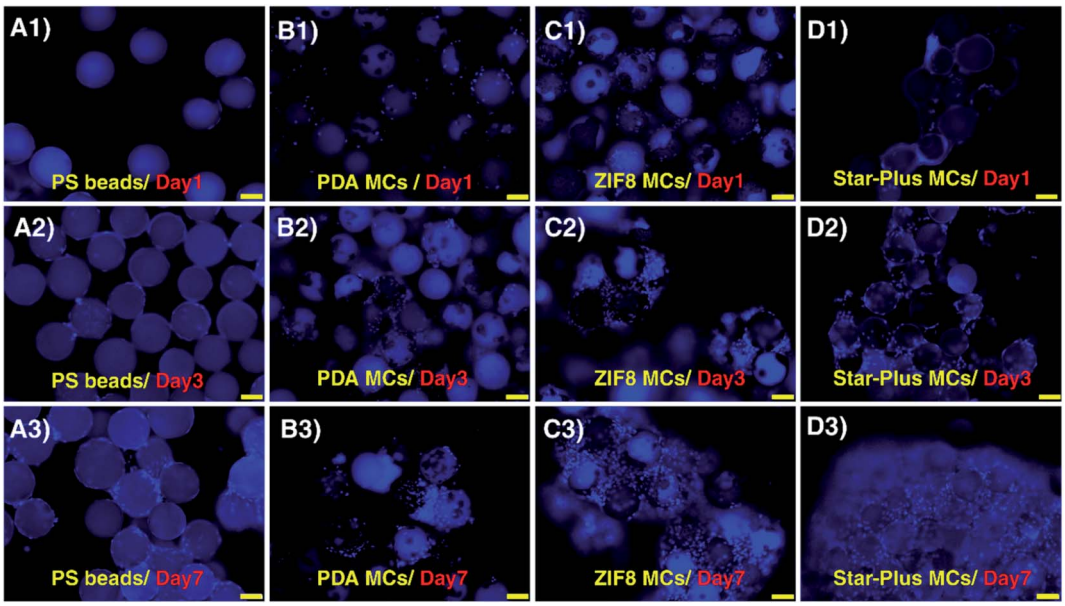

Fig. 4 Fluorescent microscopy images of hADSCs attachment and growth on MCs under static condition over 7 days. PS beads: (A1) day 1, (A2) day 3, (A3) day 7. PDA MC: (B1) day 1, (B2) day 3, (B3) day 7. ZIF8 MC: (C1) day 1, (C2) day 3, (C3) day 7. Star-Plus MC: (D1) day 1, (D2) day 3, (D3) day 7. Cell adhesion increased by coating PDA and PDA/ZIF8 on the surface of PS beads. ZIF8 MC enabled to support and proliferate cells with high efficiency. The nucleus was stained with DAPI. Scale bar: 100 μm.

cell attachment and growth efficiency of cells on ZIF8 MCs were evaluated under static conditions. With this in mind, cell seeding was conducted with MCs with different surface properties such as PS beads, PDA MCs, and Star-Plus MCs.

Fluorescent microscopy images of static culture condition indicate a few numbers of attached cells on PS beads on the first day which subsequently show the lowest cell growth efficiency on the 3rd and 7th day of cell culture (Fig. 4A1–A3). In contrast, PDA coating enhanced hADSCs cell attachment and growth due to the intrinsic cell adherent properties of PDA[47] (Fig. 4B1–B3). Star-Plus MCs promoted the attachment and expansion of negatively charged hADSCs due to its positive net charge (Fig. 4D1–D3). ZIF8 MCs reached similar cell attachment level and growth compared with Star-Plus MCs as a positive control (Fig. 4C1–C3).

Aggregates of cells-MCs were observed in PDA, Star-Plus, and ZIF8 MCs. The size of the aggregates enlarged over time. The large aggregates of cells-MCs may result from the high cell attachment capacity and insufficient space for cell spreading. As ultra-low adherent wells were used for static culture, cells could only attach and expand on the surface of MCs. Once MCs surfaces are fully covered by cells, cells begin to adhere to the extracellular matrix produced by other cells, leading to cell aggregation. These aggregates lead to cell necrosis and low viable cell yield.[48] However, agglomeration can be decreased by suspending MCs and cells in stirred bioreactors and optimizing cell culture parameters.

3.3. hADSCs culture in the dynamic condition

The previous results demonstrate ZIF8 MCs can support a high level of cell growth in 2D cell culture. However, MCs culture under static conditions has limitations in producing significant numbers of cells. Therefore, we explore the feasibility of ZIF8 MCs in a stirred culture system by evaluation of cell attachment, growth, and maintaining multilineage differentiation potential.

3.3.1 hADSCs attachment and growth on ZIF8 MCs. The capacity of carriers for appropriate cell adherence and growth are the most important factors in designing MCs, which are affected by surface properties such as roughness, zeta potential, functional groups, surface free energy, stiffness, and wettability.[56] To investigate the effect of surface properties of MCs in hADSCs attachment and growth, first, the surface occupancy of MCs by cells was studied by using confocal microscopy. Confocal images of MCs over different days are shown in Fig. 5. Star-Plus MCs supported a high level of cell attachment and growth over time. The reason for high cell attachment and growth can be attributed to the surface chemistry and positive surface charge of Star-Plus MCs (+33.2 mV) (Table 1). Functional groups are another important factor which affects cell attachment and growth of MCs. Cell adhesion and spreading increase with modification of the surface with amine groups. A moderate level of primary cell adhesion was observed on the surface of PS due to the presence of primary amines present on the PS beads (Fig. 5A1). However, there was no significant enhancement in the number of cells at day 3 and 7 (Fig. 5A2 and A3).

By comparison, cell attachment and growth increased by coating PDA on the surface of PS beads. This result highlights the impact of quinone groups on the surface of PDA MCs which promote a larger amount of protein attachment and subsequently, higher cell attachment and growth in PDA MCs.[57] Surprisingly, after coating ZIF8 thin film on the surface of PDA MCs, cell attachment and proliferation further increased

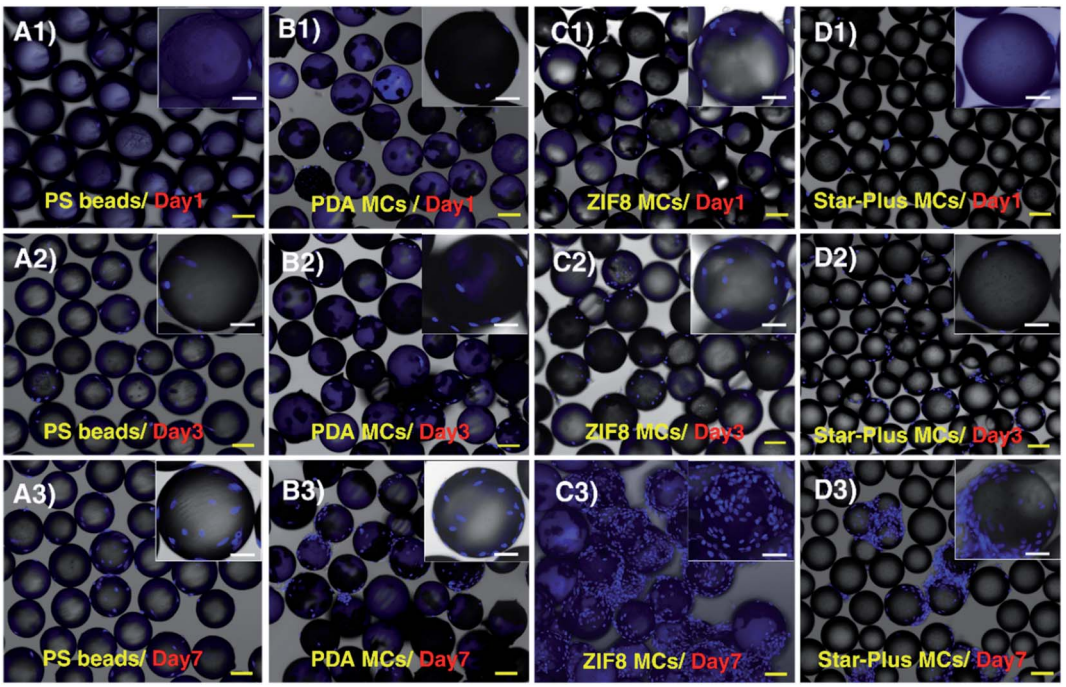

Fig. 5 Confocal microscopy images of MCs in dynamic conditions. PS beads: (A1) day 1, (A2) day 3, (A3) day 7. PDA MC: (B1) day 1, (B2) day 3, (B3) day 7. ZIF8 MC: (C1) day 1, (C2) day 3, (C3) day 7. Star-Plus MCs: (D1) day 1, (D2) day 3, (D3) day 7. The images of PS beads and PDA MCs in different days of culture indicate cell proliferation enhanced by PDA coating. Using ZIF8 thin film layer in the fabrication of MCs show a significant increase in cell attachment and growth compared to PS beads and PDA MCs. The nuclei were stained with DAPI. Yellow scale bars indicate 100 μm, and white scale bars indicate 50 μm.

equivalent to Star-Plus MCs. Aggregates of cells-MCs was observed upon the proliferation of cell on ZIF8 on the day 7. MCs. Fig. 5C shows, cell density increased significantly at the end of the culture period, and ZIF8 MCs were fully covered by cells. The number of cells harvested from MCs at the end of the culture period (Fig. 6A) was in agreement with the number of

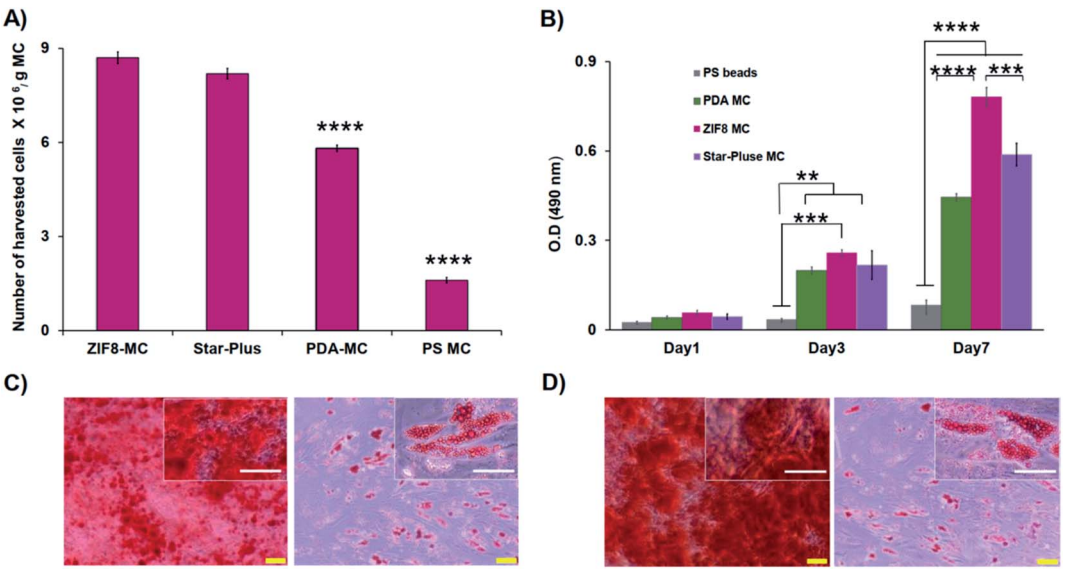

Fig. 6 Potential of proliferation and differentiation of hMSCs cultured in MCs in 3D cell culture. (A) Total viable cell density obtained by 3D expansion of cells on PS MCs, PDA MCs, ZIF8 MCs, and Star-Plus MCs after 7 days of culture. ZIF8 MCs supported a high level of ADSCs (5.8 fold expansion). (B) Analysis of cell attachment and growth on the surface of PS beads, PDA MCs, ZIF8 MCs, and Star-Plus MCs using MTS assay. PDA and ZIF8 coating improve cell attachment and growth of PS beads with a significant difference. Multipotency assay of harvested hADSCs from (C) PDA MCs (osteoblasts, left panel) (adipocytes, right panel) and (D) (osteoblasts, left panel) (adipocytes, right panel). PDA and ZIF8 MCs retained their differential potential under dynamic conditions. Data represented as mean ± SEM, from four independent experiments, numerical variables were statistically evaluated by one-way ANOVA test.*P value < 0.05 considered significant. The result for the above indicates a high significant **P value < 0.01, ***P value < 0.001, ****P value < 0.0001.

cells observed by confocal microscopy. PS beads did not promote cell growth and produced only 1.6×10^6 cells per g MCs which was much lower than the number of cells harvested from Star-Plus MCs (8.2×10^6 cells per g MCs, 5.4-fold increase relative to the amount of inoculated cells). After coating PS beads with PDA/PEI, cell yield increased to 5.8×10^6 cells per g MCs with 3.9-fold proliferation. Remarkably, the cell yield of ZIF8 MCs enhanced significantly against the PS beads, and PDA MCs (P value < 0.0001) with total cell density 8.8×10^6 cells per g MCs and 5.8-fold cell proliferation. On the other hand, ZIF8 MCs showed a slight increase in cell harvested yield compared with Star-Plus MCs. It is plausible that the slight difference between these two MCs results from their different density. Indeed, ZIF8 MCs possess higher density against Star-Plus MCs which cause cells-MCs aggregation and consequently reducing cell yield. It is very likely by using beads with lower density, cell yield increase even more.

Further monitoring of cell growth on the MCs surface was conducted with MTS assay (Fig. 6B). The MTS assay features the reduction of a tetrazolium compound with viable cells to produce colored formazan compounds soluble in media. The absorbance of media at 490 nm can be used for quantification of viable cells. By analyzing the results obtained from MTS assay, it can be observed that cell metabolic rate increased for the positive control (Star-Plus MCs) during 7 days of culture, and ZIF8 MCs follow the same trend. Therefore, ZIF8 coating did not present cytotoxic effects, demonstrating that ZIF8 MCs are biocompatible. It is noteworthy, cell attachment and growth of PS beads were significantly lower than other MCs. In comparison, initial cell attachment increased after PDA/PEI coating on the beads, and as a result, cell growth and proliferation were enhanced significantly compared with PS beads. After coating ZIF8 on PDA MCs, cell proliferation efficiency raised over time and cell metabolic activity increased significantly with reference to other MCs on 7^{th} day of culture (P value < 0.0001).

The greater cell yield and cell metabolic activity obtained with ZIF8 MCs is a result of the inherent surface properties of ZIF8 MCs, proven with zeta potential, AFM, BET, SEM, and contact angle characterization. Comparing the results obtained by the characterization of MCs and MC cell culture, we can conclude firstly that coating ZIF8 on the surface of PDA MCs reduced the magnitude of negative zeta potential and subsequently improve cell viability and proliferation. Secondly, the chemical features of ZIF8 MCs, such as abundant nitrogen functional groups assist cell attachment and growth.[58] Thirdly, BET and AFM results show that ZIF8 coating increases the surface area and roughness of MCs. Due to the formation of microporous ZIF8 crystals on the surface of MCs, a larger surface area for cell adhesion is provided. Furthermore, nanoscale topography of ZIF8 MCs affects cell adhesion and proliferation.[59] AFM images indicate that the surface of ZIF8 MCs possess nano roughness. Nanoscale features of ZIF8 MCs can mimic the extracellular matrix proteins (ECM). Indeed, ECM proteins contain nanostructured topography and contribute to cell–matrix signaling and consequently enhance cell attachment and adhesion.[59] Surface free energy is another important factor which has a positive effect on cell spreading, attachment, and cell growth.[60] ZIF8 MCs with higher surface free energy compared with other MCs exhibit better cell attachment and proliferation. Lastly, the results obtained by expanding cells on various MCs verify that hADSCs cell attachment and proliferation enhance on the surface MCs with greater hydrophilicity and roughness. These results are similar to those reported, which indicate hADSCs attachment and growth are better on hydrophilic and rough substrates compared with hydrophobic and smooth surfaces.[61]

3.3.2 Multilineage differentiation potential of MC-derived cells. In order to confirm and PDA MCs and ZIF8 MCs maintain hADSCs multipotency, harvested cells were cultured in differentiation medium and then stained with adipogenesis and osteogenesis markers (Fig. 6C and D respectively). Formation of bright red stain calcium deposits stained by Alizarin Red S confirmed osteoblastic phenotype of cells. In addition, the presence of red lipid droplets stained by Oil Red O indicates adipocyte phenotype.

4 Conclusion

Here was demonstrate the promising application of ZIF8 in surface modification of MCs. We found out ZIF8 thin film layer coating could effectively promote surface property of PS beads such as wettability, roughness, surface charge, and surface free energy to stimulate cell attachment and growth in both dynamic and static cell culture conditions. The ZIF8 MCs were biocompatible and maintained their differentiate potential in 3D cell culture. They achieved greater cell growth and cell yield compared with other tested MCs. ZIF8 MCs were fabricated by modifying PS beads with ZIF8/PDA/PEI at room temperature without using any toxic or organic solvents. A ZIF8 crystal layer was formed on the surfaces of MCs, possessing the mechanical properties necessary to support cells in bioreactors. The proposed method for fabrication of MCs is non-toxic, cost-effective, and straightforward that may be adopted as a generalized method for converting non-wetting beads to bioactive and tunable MCs with high cell adhesion and viability. Importantly, the unique features of ZIF8 such as high tunability and drug loading capacity, make them a powerful tool for future clinical therapies and tissue engineering.

Data availability

The raw/processed data required to reproduce these findings cannot be shared at this time as the data also forms part of an ongoing study.

Conflicts of interest

There are no conflicts to declare.

Acknowledgements

M. E. W. would like to acknowledge the support of the Australian Research Council through Discovery Project Grants

(DP170103704 and DP180103003) and the National Health and Medical Research Council through the Career Development Fellowship (APP1143377). We would like to thank the valuable assistance of Dr Alf Garcia-Bennett in BET surface area analysis. We also acknowledge Regeneus for generous funding of this research.

References

1 R. E. Fitzsimmons, M. S. Mazurek, A. Soos and C. A. Simmons, *Stem Cells Int.*, 2018, **2018**, 8031718.
2 Y. Jiang, B. N. Jahagirdar, R. L. Reinhardt, R. E. Schwartz, C. D. Keene, X. R. Ortiz-Gonzalez, M. Reyes, T. Lenvik, T. Lund and M. Blackstad, *Nature*, 2002, **418**, 41–49.
3 M. Sekula and E. K. Zuba-Surma, *Biomaterials in Regenerative Medicine*, 2018, pp. 361–375.
4 C. Vinatier and J. Guicheux, *Ann. Phys. Rehabil. Med.*, 2016, **59**, 139–144.
5 A. A. Rizvanov, J. Persson, F. Şahin, S. Bellusci and P. J. Oliveira, *Stem Cells Int.*, 2016, **2016**, 3157365.
6 J. Kobolak, A. Dinnyes, A. Memic, A. Khademhosseini and A. J. M. Mobasheri, *Methods*, 2016, **99**, 62–68.
7 A. I. Caplan, *J. Cell. Physiol.*, 2016, **231**, 1413–1416.
8 A.-M. Yousefi, P. F. James, R. Akbarzadeh, A. Subramanian, C. Flavin and H. J. Oudadesse, *Stem Cells Int.*, 2016, **2016**, DOI: 10.1155/2016/6180487.
9 Z. Mahmoudi, J. Mohammadnejad, S. Razavi Bazaz, A. Abouei Mehrizi, M. Saidijam, R. Dinarvand, M. Ebrahimi Warkiani and M. Soleimani, *Carbohydr. Polym.*, 2019, **229**, 115551.
10 Z. Hesari, M. Soleimani, F. Atyabi, M. Sharifdini, S. Nadri, M. Ebrahimi Warkiani, M. Zare and R. Dinarvand, *J. Biomed. Mater. Res., Part A*, 2016, **104**, 1534–1543.
11 H. D. Zomer, A. S. Vidane, N. N. Goncalves and C. E. Ambrosio, *Stem Cells Cloning: Adv. Appl.*, 2015, **8**, 125.
12 A. K.-L. Chen, S. Reuveny and S. K. W. Oh, *Biotechnol. Adv.*, 2013, **31**, 1032–1046.
13 D. Kuah, S. Sivell, T. Longworth, K. James, A. Guermazi, F. Cicuttini, Y. Wang, S. Craig, G. Comin and D. Robinson, *J. Transl. Med.*, 2018, **16**, 49.
14 A. Tyndall and A. J. Uccelli, *Bone Marrow Transplant.*, 2009, **43**, 821.
15 S. Wu, Y. Suzuki, Y. Ejiri, T. Noda, H. Bai, M. Kitada, K. Kataoka, M. Ohta, H. Chou and C. J. Ide, *J. Neurosci. Res.*, 2003, **72**, 343–351.
16 M. Derakhshani, H. Abbaszadeh, A. A. Movassaghpour, A. Mehdizadeh, M. Ebrahimi Warkiani and M. Yousefi, *Life Sci.*, 2019, **232**, 116598.
17 I. Ullah, R. B. Subbarao and G. J. Rho, *Biosci. Rep.*, 2015, **35**, e00191.
18 H. Tavassoli, S. N. Alhosseini, A. Tay, P. P. Chan, S. K. W. Oh and M. Ebrahimi Warkiani, *Biomaterials*, 2018, **181**, 333–346.
19 A. T.-L. Lam, A. K.-L. Chen, S. Q.-P. Ting, S. Reuveny and S. K.-W. Oh, *Biochem. Biophys. Res. Commun.*, 2016, **473**, 764–768.
20 M. A. Raoufi, S. Razavi Bazaz, H. Niazmand, O. Rouhi, M. Asadnia, A. Razmjou and M. Ebrahimi Warkiani, *Soft Matter*, 2020, **16**, 2448–2459.
21 R. Moloudi, S. Oh, C. Yang, K. L. Teo, A. T.-L. Lam, M. Ebrahimi Warkiani and M. W. Naing, *Sci. Rep.*, 2018, **8**, 12481.
22 J. Yang, P. Guertin, G. Jia, Z. Lv, H. Yang and D. Ju, *AMB Express*, 2019, **9**, 70.
23 F. Abeille, F. Mittler, P. Obeid, M. Huet, F. Kermarrec, M. Dolega, F. Navarro, P. Pouteau, B. Icard and X. Gidrol, *Lab Chip*, 2014, **14**, 3510–3518.
24 R. Moloudi, S. Oh, C. Yang, K. L. Teo, A. T. L. Lam, M. Ebrahimi Warkiani and M. Win Naing, *Biotechnol. J.*, 2019, **14**, 1800674.
25 M. Ravi, V. Paramesh, S. Kaviya, E. Anuradha and F. P. Solomon, *J. Cell. Physiol.*, 2015, **230**, 16–26.
26 Y. Martin, M. Eldardiri, D. J. Lawrence-Watt and J. R. Sharpe, *Tissue Eng., Part B*, 2011, **17**, 71–80.
27 B. Li, X. Wang, Y. Wang, W. Gou, X. Yuan, J. Peng, Q. Guo and S. J. Lu, *J. Orthop. Transl.*, 2015, **3**, 51–57.
28 A. J. N. Van Wezel, *Nature*, 1967, **216**, 64.
29 S. Sart, S. N. Agathos and Y. J. Li, *Biotechnol. Prog.*, 2013, **29**, 1354–1366.
30 S. Hinderer, S. L. Layland and K. J. Schenke-Layland, *Adv. Drug Delivery Rev.*, 2016, **97**, 260–269.
31 P. Gupta, M.-Z. Ismadi, P. J. Verma, A. Fouras, S. Jadhav, J. Bellare and K. Hourigan, *Cytotechnology*, 2016, **68**, 45–59.
32 M. S. Croughan, J. F. Hamel and D. I. Wang, *Biotechnol. Bioeng.*, 2000, **67**, 841–852.
33 R. A. Perez, K. Riccardi, G. Altankov and M.-P. Ginebra, *J. Tissue Eng.*, 2014, **5**, DOI: 10.1177/2041731414543965.
34 Q. Zan, C. Wang, L. Dong, P. Cheng and J. Tian, *Appl. Surf. Sci.*, 2008, **255**, 401–403.
35 T. K.-P. Goh, Z.-Y. Zhang, A. K.-L. Chen, S. Reuveny, M. Choolani, J. K. Y. Chan and S. K. W. Oh, *BioRes. Open Access*, 2013, **2**, 84–97.
36 M. Kuterbekov, P. Machillot, P. Lhuissier, C. Picart, A. M. Jonas and K. Glinel, *Acta Biomater.*, 2018, **75**, 300–311.
37 J.-H. Park, R. A. Pérez, G.-Z. Jin, S.-J. Choi, H.-W. Kim and I. B. Wall, *Tissue Eng., Part B*, 2013, **19**, 172–190.
38 H.-C. Zhou, J. R. Long and O. M. Yaghi, *Chem. Rev.*, 2012, **112**, 673–674.
39 H. Wang, F. X. Yin, N. Liu, R. H. Kou, X. B. He, C. J. Sun, B. H. Chen, D. J. Liu and H. Q. Yin, *Adv. Funct. Mater.*, 2019, 1901531.
40 Y. Liu, R. Wang, T. Zhang, S. Liu and T. Fei, *J. Colloid Interface Sci.*, 2019, **541**, 249–257.
41 B. Chang, Y. Yang, H. Jansen, F. Ding, K. Mølhave and H. Sun, *Adv. Mater. Interfaces*, 2018, **5**, 1701270.
42 X. Zhao, X. Fang, B. Wu, L. Zheng and N. F. Zheng, *Sci. China: Chem.*, 2014, **57**, 141–146.
43 F. Fu, B. Zheng, L.-H. Xie, H. Du, S. Du and Z. Dong, *Crystals*, 2018, **8**, 367.
44 R. Riccò, W. Liang, S. Li, J. J. Gassensmith, F. Caruso, C. Doonan and P. Falcaro, *ACS Nano*, 2018, **12**, 13–23.
45 K. Liang, J. J. Richardson, J. Cui, F. Caruso, C. J. Doonan and P. Falcaro, *Adv. Mater.*, 2016, **28**, 7910–7914.

46 M. X. Wu and Y. W. Yang, *Adv. Mater.*, 2017, **29**, 1606134.
47 G. Chen, B. Yu, C. Lu, H. Zhang, Y. Shen and H. Cong, *CrystEngComm*, 2018, **20**, 7486–7491.
48 Q. Wu, M. Niu, X. Chen, L. Tan, C. Fu, X. Ren, J. Ren, L. Li, K. Xu and H. Zhong, *Biomaterials*, 2018, **162**, 132–143.
49 A. Razmjou, M. Asadnia, O. Ghaebi, H.-C. Yang, M. Ebrahimi Warkiani, J. Hou and V. Chen, *ACS Appl. Mater. Interfaces*, 2017, **9**, 38076–38080.
50 M. Mohammad, A. Razmjou, K. Liang, M. Asadnia and V. Chen, *ACS Appl. Mater. Interfaces*, 2018, **11**, 1807–1820.
51 S. K. Madhurakkat Perikamana, J. Lee, Y. B. Lee, Y. M. Shin, E. J. Lee, A. G. Mikos and H. Shin, *Biomacromolecules*, 2015, **16**, 2541–2555.
52 X. Ruan, X. Zhang, Z. Zhou, X. Jiang, Y. Dai, X. Yan and G. He, *Sep. Purif. Technol.*, 2019, **214**, 95–103.
53 R. N. Wenzel, *Ind. Eng. Chem.*, 1936, **28**, 988–994.
54 J. Fu, Z. Chen, M. Wang, S. Liu, J. Zhang, J. Zhang, R. Han and Q. Xu, *Chem. Eng.*, 2015, **259**, 53–61.
55 C.-s. Wu, Z.-h. Xiong, C. Li and J.-m. Zhang, *RSC Adv.*, 2015, **5**, 82127–82137.
56 M. Ferrari, F. Cirisano and M. C. Morán, *Colloids Interfaces*, 2019, **3**, 48.
57 Y. Ding, M. Floren and W. Tan, *Biosurf. Biotribol.*, 2016, **2**, 121–136.
58 K. Webb, V. Hlady and P. A. Tresco, *J. Biomed. Mater. Res.*, 1998, **41**, 422–430.
59 C. J. Bettinger and R. Langer, *Angew. Chem., Int. Ed.*, 2009, **48**, 5406–5415.
60 J. Schakenraad, H. Busscher, C. R. Wildevuur and J. J. Arends, *J. Biomed. Mater. Res.*, 1986, **20**, 773–784.
61 H. Ahn, I. Lee, H. Lee and M. S. Kim, *Int. J. Mol. Sci.*, 2014, **15**, 2075–2086.